Chinese Chemical Letters 32 (2021) 2207–2211

Contents lists available at ScienceDirect

Chinese Chemical Letters

journal homepage: www.elsevier.com/locate/cclet

Communication

Covalent organic framework stabilized CdS nanoparticles as efficient visible-light-driven photocatalysts for selective oxidation of aromatic alcohols

Kaiyue Zhang[1], Guilong Lu[1], Zuoshuai Xi, Yaqiong Li, Qingjie Luan, Xiubing Huang*

Beijing Advanced Innovation Center for Materials Genome Engineering, Beijing Key Laboratory of Function Materials for Molecule & Structure Construction, School of Materials Science and Engineering, University of Science and Technology Beijing, Beijing 100083, China

ARTICLE INFO

Article history:
Received 28 October 2020
Received in revised form 16 November 2020
Accepted 11 December 2020
Available online 2 March 2021

Keywords:
Covalent organic frameworks
CdS nanoparticles
Photocatalyst
Selective alcohol oxidation
Visible light
Green organic synthesis

ABSTRACT

Noble-metal-free photocatalysts with high and stable performance provide an environmentally-friendly and cost-efficient route for green organic synthesis. In this work, CdS nanoparticles with small particle size and different amount were successfully deposited on the surface of covalent organic frameworks (COFs). The deposition of suitable content of CdS on COFs could not only modify the light adsorption ability and the intrinsic electronic properties, but also enhance the photocatalytic activity and cycling performance of CdS for the selective oxidation of aromatic alcohols under visible light. Especially, COF/CdS-3 exhibited the highest yield (97.1%) of benzaldehyde which is approximately 2.5 and 15.9 times as that of parental CdS and COF, respectively. The results show that the combination of CdS and COF can improve the utilization of visible light and the separation of photo-generated charge carriers, and COF with the π-conjugated system as supports for CdS nanoparticles could provide efficient electron transport channels and improve the photocatalytic performance. Therefore, this kind of COF-supported photocatalysts with accelerated photo-induced electrons and charge-carrier separation between semiconductors possesses great potentials in future green organic synthesis.

In recent years, cadmium sulfide has been widely used in the field of photocatalysis because of its narrow band width and appropriate conduction band/valence band potential, such as water splitting, photoreduction of carbon dioxide, and photocatalytic organic reactions [1–3]. However, it has some obvious defects that limit its catalytic efficiency in specific applications, such as small specific surface area, high photo-generated electron and hole recombination rate, and easy to be corroded by light during the reaction. Although in recent years, the photocatalytic performance of CdS can be improved to some extent by changing its morphology (nanorod, nanoparticle, flower-like, *etc.*) [4–6], or adjusting its photogenerated carrier current by doping with other elements or combining with other types of semiconductors [7,8], but the current strategies are not particularly satisfactory.

Due to the existence of extensive π-conjugated system and promoted electron transfer ability, conjugated polymers have been applied in photocatalytic fields, such as CdS@C_3N_4 [9–11]. Covalent organic frameworks (COFs), which constructed of small organic molecules and covalent bonds, can be emerged as an effective photo-generated carrier transport channel to promote the separation rate of photo-generated electrons and holes because of their easy adjustment of the electronic structure [12–15]. In addition, the excellent properties of COFs (*e.g.*, tunable pore size, and extended absorption spectrum) have also enabled COFs as effective photocatalysts or photocatalyst supports for CdS in photocatalytic hydrogen evolution [16–19].

Recently, photocatalytic organic transformation has attracted increasing attentions due to its merits of environmentally-friendly, cost-effective and high selectivity for targeted products, and various kinds of photocatalysts (*e.g.*, MIL-125(Ti)-NH_2 [20], Rh-doped $SrTiO_3$ [21], AuPd/conjugated microporous polymer [22]) have been investigated for visible-light-driven organic synthesis [23]. Even though CdS has also been reported as visible-light-driven photocatalysts for selective oxidation of benzyl alcohol, its photo-corrosion still limits its long-term stability [24–26]. Driven by the high surface areas, tunable pore size, extended π-conjugated system, efficient electron transport ability and visible-light

* Corresponding author.
E-mail address: xiubinghuang@ustb.edu.cn (X. Huang).
[1] These authors contributed equally to this work.

https://doi.org/10.1016/j.cclet.2020.12.021

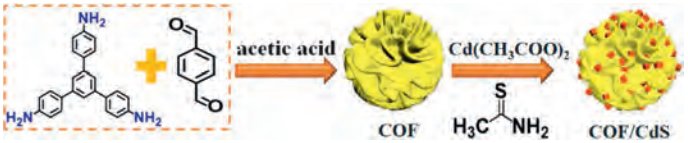

Scheme 1. Illustration of the synthesis process of COF/CdS photocatalyst.

responsive ability, COFs or COFs-based photocatalysts recently were also reported for photocatalytic organic transformation [27–29].

In this work, a series of COF/CdS photocatalysts with different cadmium sulfide contents deposited on the surface of COF were prepared. The utilization ability of visible light and the transfer efficiency of photo-generated carriers were characterized. Based on the results of the catalytic oxidation of benzyl alcohol, it was verified that COF/CdS photocatalysts with CdS nanoparticles deposited on the surface of COFs not only have a high specific surface area, a multi-stage special pore structure, an efficient photo-generated electron transport system, but also can effectively inhibit the photocorrosion of CdS. This research provides a good idea for the design of future COF-based photocatalysts.

First, pure COF was prepared using terephthalaldehyde and 1,3,5-tris (4-aminophenyl) benzene as precursor and acetic acid as catalyst according to our previous literature, as shown in Scheme 1 [29]. In order to obtain COF/CdS catalysts with different CdS amounts, different mass ratios of cadmium acetate, thioacetamide and COF were added into ethanol solutions and COF/CdS composites were formed after reaction at 80 °C for 40 min under continuous stirring. According to the increased content of CdS in the composite, the final products were named as COF/CdS-1, COF/CdS-2, COF/CdS-3 and COF/CdS-4, respectively. Pure CdS was prepared in the synthesis procedure similar to the cadmium sulfide deposition experiment but without COF. Detailed experimental procedure was shown in the Supporting information.

X-ray diffraction (XRD) is used to check the phase structures of CdS, COF and COF/CdS-3. As shown in Fig. 1a, the broad characteristic diffraction peaks belong to cubic-phase CdS (JCPDS No. 90-0440), which proves that CdS nanoparticle crystals have been successfully synthesized from cadmium acetate and thioacetamide in a hot ethanol solution [30]. After the CdS nanoparticles are deposited on the surface of COF, the intensity of the diffraction peaks of CdS in COF/CdS-3 (Fig. 1a) becomes weaker, suggesting their small content and small nanoparticle size. The characteristic peaks belonging to the (111), (220) and (311) crystal planes of cubic-phase CdS can be clearly observed, which proves the successful deposition of CdS nanoparticles on the surface of COF. As shown in Fig. 1b, pure COF exhibits characteristic diffraction peaks at low diffraction angle range, demonstrating the uniform mesoporous and microporous structure of COFs, while there is only one sharp diffraction peak with lower intensity at low diffraction angle range for COF/CdS-3 maybe due to the fill of CdS nanoparticles and/or nanoclusters in the pores.

The morphologies of the synthesized samples were analyzed by transmission electron microscope (TEM) and scanning electron microscope (SEM). Fig. S1a (Supporting information) shows that the surface of pure COF microspheres has a large number of two-dimensional folds, which could provide a large number of suitable sites for CdS nanoparticle deposition. After the deposition of CdS, it can be found that CdS nanoparticles with a small size appear on the surface of the COF microspheres in COF/CdS-3 (Figs. 1c and d) and the particle size of CdS slightly increased with the increasing CdS content (Fig. S1 in Supporting information). Compared with the size of pure CdS (Fig. S1f), the decrease in the CdS nanoparticle size after deposition can be attributed to the lower nucleation energy required for heterogeneous nucleation [31,32]. The load amounts of CdS in COF/CdS-1, COF/CdS-2, COF/CdS-3 and COF/CdS-4 samples were determined to be 8.63 wt%, 17.03 wt%, 26.81 wt% and 29.70 wt%, respectively based on the Inductively Coupled Plasma Optical Emission Spectrometry (ICP-OES) results.

According to the Fourier transform infrared (FI-IR) spectrum (Fig. 2a), it is found that in the range of 900–1750 cm^{-1}, there are mainly characteristic peaks that belong to COF, including chemical bonds such as C=N, C=C, N—H. The characteristic peak of C=N bond located near 1700 cm^{-1} belongs to the imine structure, and its intensity increases as the proportion of COF in the complex increases, proving the successful synthesis of COF.

In the X-ray photoelectron spectroscopy (XPS) survey curve (Fig. S2a in Supporting information), the COF/CdS-3 sample contains only the four elements C, N, Cd and S, and no other

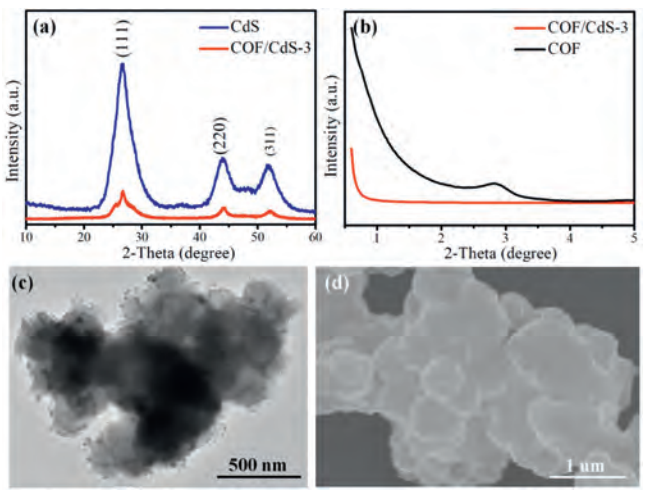

Fig. 1. (a) Powder XRD patterns of CdS and COF/CdS-3. (b) Small-angle XRD of COF and COF/CdS-3. (c) TEM and (d) SEM images of COF/CdS-3.

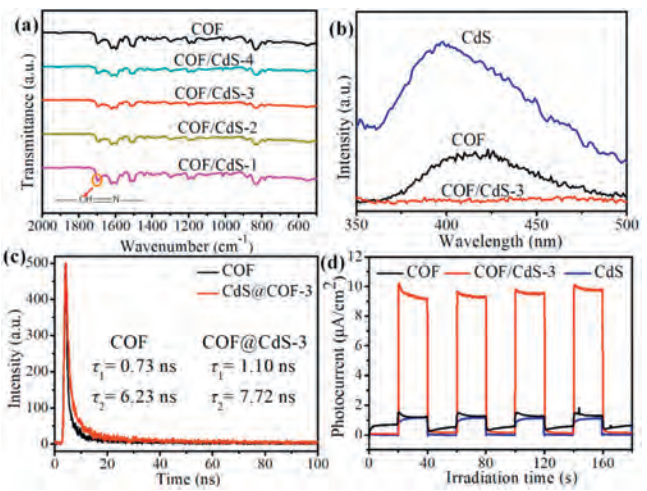

Fig. 2. FT-IR spectrum (a), fluorescence emission spectrum (b), fluorescence lifetime spectrum (c) and photocurrent test results (d) of as-prepared samples.

impurity elements are present. In the C 1s XPS spectrum (Fig. S2b in Supporting information), the characteristic peaks corresponding to C=C (286.1 eV) of sp^2 hybridization in the benzene ring, C=N (285.1 eV) in the imine structure and the C—N (284.3 eV) in unreacted 4-aminophenyl groups can be clearly observed. In the N 1s XPS spectrum (Fig. S2c in Supporting information), the characteristic peaks (400.0 eV and 398.9 eV) corresponding to pyrrole N and pyridine N in the COF structure can be clearly observed in COF/CdS-3, and there is no obvious shift in the N 1s spectrum between COF/CdS-3 and pure COF maybe due to the small amount of CdS on its surface. According to the XPS spectrum of Cd 3d (Fig. S2d in Supporting information), the characteristic peaks of the two 3d orbits belong to Cd^{2+}. In the S 2p XPS spectrum (Fig. S2e in Supporting information), the two distinct characteristic peaks of the S $2p_{1/2}$ and S $2p_{3/2}$ orbits confirmed the S^{2-} state in the complex, indicating the existence of CdS in COF/CdS-3. Compared with those of pure CdS, the binding energies of Cd 3d and S 2p positively shifted in COF/CdS-3, indicating there is a strong interaction and not just simple physical content between COF microspheres and CdS nanoparticles [19,33]. In addition, the XPS valence band (VB) spectrum was used to obtain the valence band potential information of COF and CdS (Fig. S3 in Supporting information). The valence band potentials of COF and CdS are approximately 1.248 eV and 1.490 eV, respectively.

According to the UV–vis spectrum (Fig. S4a in Supporting information), the visible light response ability of composites is gradually enhanced as the content of deposited CdS increases. After calculation of the UV–vis spectrum, the band gaps corresponding to the photocatalysts can be obtained from the transferred $(Ah\upsilon)^2$-$h\upsilon$ curves. From Fig. S4b (Supporting information), the band gaps of COF, COF/CdS-1, COF/CdS-2, COF/CdS-3, COF/CdS-4 and CdS are 2.565, 2.575, 2.560, 2.523, 2.472 and 2.412 eV, respectively. Combined with the VB potentials of COF and CdS, the conduction bands of COF and CdS can be calculated to be −1.317 eV and −0.922 eV, respectively, which construct a typical type-II heterojunction for improving the separation and transfer of photo-generated charge carriers [34].

Fluorescence spectroscopy is an important characterization method for analyzing the photo-generated carrier recombination efficiency. As shown in Fig. 2b, COF and CdS have strong fluorescence emission peaks, indicating that a large number of photo-generated electrons and holes recombine in pure COF and CdS, and the fluorescence intensity is obvious weaker when the two are combined. The decrease is mainly due to the efficient migration of photo-generated electrons from COF to CdS, which inhibits the recombination of a large number of charge carriers. The fluorescence lifetime generally refers to the average time required for the excited state electrons to go from the excited state to the ground state, so a longer fluorescence lifetime means the possibly higher usage efficiency of photogenerated electrons, maybe leading to higher photocatalytic performance. As shown in Fig. 2c, COF/CdS-3 has a longer fluorescence lifetime than pure COF, confirming that COF/CdS-3 has a stronger carrier migration ability. In addition, compared with individual CdS and COF, the photocurrent intensity of COF/CdS-3 catalyst is obviously stronger, as shown in Fig. 2d, which proves that the combination of CdS nanoparticles and COF microspheres improves the light response ability and the transfer of charge carriers.

The selective oxidation of benzyl alcohol was selected as a probe experiment to test the photocatalytic activity of the catalysts. The catalytic results are summarized in Table 1. The products of all catalysts are only benzaldehyde and no other by-products (*e.g.*, benzoic acid) were detected, indicating the excellent selectivity. The pure CdS and COF exhibited 38.3% and 6.1% conversion of benzyl alcohol (Entries 1 and 2), respectively. After the combination of COF microspheres and CdS nanoparticles, the

Table 1
Catalytic results of photocatalytic oxidation of benzyl alcohol.[a]

Entry	Catalyst	Conversion (%)	Selectivity (%)
1	CdS	38.3	99.9
2	COF	6.1	99.9
3	COF/CdS-1	41.3	99.9
4	COF/CdS-2	65.7	99.9
5	COF/CdS-3	97.1	99.9
6	COF/CdS-4	72.4	99.9
7[b]	COF/CdS-3	trace	–
8[c]	No catalyst	trace	–
9[d]	COF/CdS-3	trace	–
10[e]	CdS + COF	15.1	99.9

[a] Reaction conditions: 20 mg catalyst, 0.5 mmol benzyl alcohol, 2.7 mL trifluorotoluene and 0.3 mL acetonitrile, 15 h, a white light LED lamp of 5.0 W power (λ = 420−780 nm, power density ≈ 150 mW/cm^2), 1 atm O_2.
[b] Without light.
[c] Without photocatalysts.
[d] Under argon atmosphere.
[e] Physically mixed COF and CdS with similar composition to COF/CdS-3.

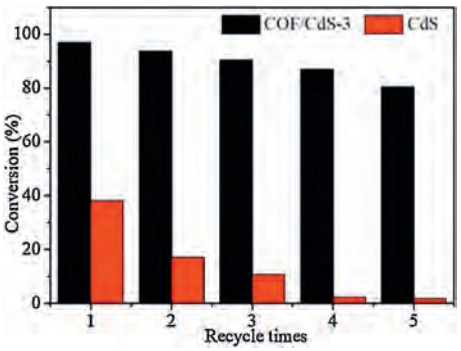

Fig. 3. Conversion of benzyl alcohol by COF/CdS-3 and CdS with cycle times.

Table 2
Catalytic results of photocatalytic oxidation of other aromatic alcohols.

Entry	Substrate	Product	Conversion (%)	Selectivity (%)
1			97.1	99.9
2			99.9	99.9
3			99.9	99.9
4			82.6	99.9
5	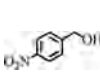		74.2	99.9
6			79.1	99.9
7			75.7	99.9

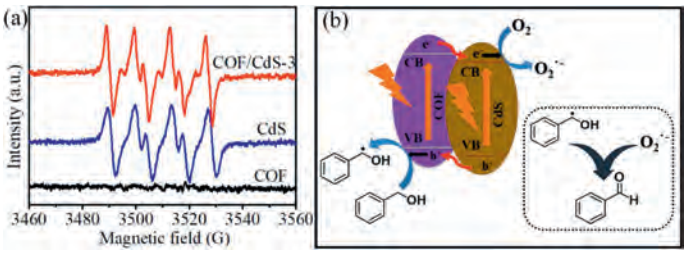

Fig. 4. (a) ESR spectra of benzyl alcohol radicals and $O_2^{\bullet-}$ radical species trapped by DMPO. (b) Proposed catalytic mechanism of the photocatalytic oxidation of benzyl alcohols over COF/CdS-3.

conversion of benzyl alcohol has been significantly improved. The conversion of benzyl alcohol firstly increased from 41.3% for COF/CdS-1 to 97.1% for COF/CdS-3, which is superior to many published results (Table S1 in Supporting information). However, furthering increasing the CdS content (*e.g.*, COF/CdS-4) would result in decreased conversion of benzyl alcohol, which may be due to the larger CdS nanoparticle size (Fig. S1e). In order to confirm that the high dispersion of CdS nanoparticles on the surface of COF did improve the efficiency of the catalyst, the photocatalytic test of the physically mixing CdS nanoparticles and COF support with similar composition to COF/CdS-3 for the oxidation of benzyl alcohol was carried out under the same reaction conditions and only 15.1% conversion was obtained (entry 10). In order to confirm that the photocatalytic reaction is indeed driven by visible light and molecular oxygen as an oxygen source, a series of control experiments (*e.g.*, without photocatalyst, without light, or under argon atmosphere) were performed. Experimental results show that catalyst, oxygen and light are essential factors in the catalytic system (entries 7–9, Table 1). The COF/CdS-3 sample after each photocatalytic test was washed and centrifuged with ethanol, dried in vacuum at 70 °C for 12 h, and then used again in the photocatalytic oxidation of benzyl alcohol under the same test conditions. According to Fig. 3, the catalytic stability of CdS nanoparticles can be greatly improved after depositing on the surface of COF. There are slight decreases to around 80% in the conversion of benzyl alcohol after 5 cycle times, which may be due to the possible photo-deactivation and loss of CdS nanoparticles on the surface of COF.

The best-performing COF/CdS-3 catalyst was selected for photocatalytic oxidation of some aromatic alcohol derivatives to test its ability to be widely used. The results in Table 2 show that this catalyst has good photocatalytic performance in the reaction of catalyzing the oxidation of various types of aromatic alcohols, even for aromatic alcohols with pendant electron groups, and secondary alcohols. For example, when aromatic alcohols with electron-withdrawing functional groups (*e.g.*, fluorine and nitro) are oxidized, the shift in electron cloud density from the benzene ring makes the catalysis more difficult, resulting in only around 80% conversion. When oxidizing some aromatic alcohols with electron-donating groups (*e.g.*, methyl and methoxy), the catalytic reaction is easier to proceed and the reaction is more thorough with almost complete conversion due to the easier activation of C–H bonds.

In order to conduct a more in-depth analysis of the photocatalytic oxidation of benzyl alcohol, according to previous reports in related literature and the results of Electronspin Resonance (ESR) tests in this work (Fig. 4a), no hydroxyl radicals were detected during the catalytic process. Only strong benzyl alcohol radicals and superoxide radicals (*e.g.*, DMPO-$O_2^{\bullet-}$) were detected with the presence of benzyl alcohol, 5,5-dimethyl-1-pyrroline *N*-oxide (DMPO) and COF/CdS-3, and in the presence of pure COF, there were no obvious free radical signals. These results show that the superoxide radicals produced by the COF/CdS-3 play a crucial role in the oxidation of benzyl alcohol. In addition, the roles of active radicals were determined by a series of radical trapping experiments using COF/CdS-3 as catalyst. When phenol was used as scavengers for holes, only 42.9% of the conversion of benzyl alcohol was maintained as compared with that without phenol. When *tert*-butanol was added as scavengers for hydroxyl radicals, 85.7% of the conversion of benzyl alcohol can be obtained as compared with that without scavengers. With combination of the ESR results, it could be inferred that superoxide radical anion and holes were the mainly active radicals for the aerobic oxidation reaction.

Based on the relative CB and VB positions of COF and CdS, control experiment results and the ESR test results, a possible catalytic reaction mechanism was proposed (Fig. 4b). CdS nanoparticles and COF effectively absorb photons to generate a large number of excited electron-hole pairs. Due to the higher CB position of COF, a large number of photo-generated electrons in the CB of COF can transfer to the CB of CdS, at where oxygen molecular can be oxidized to superoxide radical anion ($O_2^{\bullet-}$) by the photo-generated electrons. In addition, a large number of photo-generated holes have accumulated on the VB of COF, at where benzyl alcohols can be oxidized by holes to the corresponding carbon-based radicals. Finally, the carbon-based radicals react with $O_2^{\bullet-}$ radicals to form benzaldehyde.

In summary, COF-stabilized CdS nanoparticles were successfully prepared and applied as visible-light-driven photocatalysts for selective oxidation of aromatic alcohols. It is proven that the deposition of proper amount of CdS nanoparticles on COF (*e.g.*, COF/CdS-3 in this work) can significantly improve the photocatalytic activity, exhibiting a 97.1% yield of benzaldehyde which is approximately 2.5 and 15.9 times as that of parental CdS and COF. The imine-bonded COF with conjugated structures can provide efficient channels for the electron transport from COF support to the CdS, which effectively promote the separation of photo-generated electron-hole pairs, and prolong the survival time of photo-generated electrons or holes, thereby improving the photocatalytic performance. In addition, this catalyst provides some ideas for the construction of efficient COF-based photocatalysts in a certain sense.

Declaration of competing interest

The authors report no declarations of interest.

Acknowledgments

The work was supported by the National Natural Science Foundation of China (No. 51802015), National Key Research and Development Program of China (No. 2018YFB0605900), Fundamental Research Funds for the Central Universities (No. FRF-TP-20-005A3) and Interdisciplinary Research Project for Young Teachers of

USTB (Fundamental Research Funds for the Central Universities) (No. FRF-IDRY-19-020).

Appendix A. Supplementary data

Supplementary material related to this article can be found, in the online version, at doi:https://doi.org/10.1016/j.cclet.2020.12.021.

References

[1] G. Zhao, Y. Sun, W. Zhou, et al., Adv. Mater. 29 (2017) 1703258.
[2] G. Zhao, B. Hu, G.W. Busser, B. Peng, M. Muhler, ChemSusChem 12 (2019) 2795–2801.
[3] G. Zhao, W. Zhou, Y. Sun, et al., Appl. Catal. B: Environ. 226 (2018) 252–257.
[4] K. Li, M. Han, R. Chen, et al., Adv. Mater. 28 (2016) 8906–8911.
[5] Q. Li, F. Zhao, C. Qu, et al., J. Am. Chem. Soc. 140 (2018) 11726–11734.
[6] Z.R. Tang, B. Han, C. Han, Y.J. Xu, J. Mater. Chem. A 5 (2017) 2387–2410.
[7] K. Chang, M. Li, T. Wang, et al., Adv. Energy Mater. 5 (2015) 1402279.
[8] Y. Chen, J.F. Li, P.Y. Liao, et al., Chin. Chem. Lett. 31 (2020) 1516–1519.
[9] P. Chen, F. Liu, H. Ding, et al., Appl. Catal. B: Environ. 252 (2019) 33–40.
[10] H.R.S. Abdellatif, G. Zhang, X. Wang, et al., Chem. Eng. J. 370 (2019) 875–884.
[11] X. Huang, Z. Wu, H. Zheng, W. Dong, G. Wang, Green Chem. 20 (2018) 664–670.
[12] K. Geng, T. He, R. Liu, et al., Chem. Rev. 120 (2020) 8814–8933.
[13] T. Banerjee, K. Gottschling, G. Savasci, C. Ochsenfeld, B.V. Lotsch, ACS Energy Lett. 3 (2018) 400–409.
[14] N. Huang, P. Wang, D. Jiang, Nat. Rev. Mater. 1 (2016) 16068.
[15] L. Yang, D.C. Wei, Chin. Chem. Lett. 27 (2016) 1395–1404.
[16] Y. Hu, X. Hao, Z. Cui, et al., Appl. Catal. B: Environ. 260 (2020) 118131.
[17] J. Thote, H.B. Aiyappa, A. Deshpande, et al., Chem. Eur. J. 20 (2014) 15961–15965.
[18] D. Wang, X. Li, L.L. Zheng, et al., Nanoscale 10 (2018) 19509–19516.
[19] D. Wang, H. Zeng, X. Xiong, et al., Sci. Bull. 65 (2020) 113–122.
[20] Z. Wu, X. Huang, H. Zheng, et al., Appl. Catal. B: Environ. 224 (2018) 479–487.
[21] G. Zhao, G.W. Busser, C. Froese, et al., J. Phys. Chem. Lett. 10 (2019) 2075–2080.
[22] Y. Li, L. Wang, J. Low, et al., Chin. Chem. Lett. 31 (2020) 231–234.
[23] X. Wang, D. Jing, M. Ni, Sci. Bull. 62 (2017) 597–598.
[24] J.L. DiMeglio, A.G. Breuhaus-Alvarez, S. Li, B.M. Bartlett, ACS Catal. 9 (2019) 5732–5741.
[25] H. Hao, X. Lang, ChemCatChem 11 (2019) 1378–1393.
[26] X. Ning, S. Meng, X. Fu, X. Ye, S. Chen, Green Chem. 18 (2016) 3628–3639.
[27] Z. Li, Y. Zhi, P. Shao, et al., Appl. Catal. B: Environ. 245 (2019) 334–342.
[28] G. Lu, X. Huang, Z. Wu, et al., Appl. Surf. Sci. 493 (2019) 551–560.
[29] G. Lu, X. Huang, Y. Li, et al., J. Energy Chem. 43 (2020) 8–15.
[30] H. Yu, W. Zhong, X. Huang, P. Wang, J. Yu, ACS Sustain. Chem. Eng. 6 (2018) 5513–5523.
[31] Y. Cui, J. Stojakovic, H. Kijima, A.S. Myerson, Cryst. Growth Des. 16 (2016) 6131–6138.
[32] Y.S. Jun, D. Kim, C.W. Neil, Acc. Chem. Res. 49 (2016) 1681–1690.
[33] N. Liu, L. Shi, X. Han, et al., Chin. Chem. Lett. 31 (2020) 386–390.
[34] X. An, Y. Wang, J. Lin, et al., Sci. Bull. 62 (2017) 599–601.